ADVANCED ENERGY MATERIALS
www.advenergymat.de

Ultrathin MoS_2/Nitrogen-Doped Graphene Nanosheets with Highly Reversible Lithium Storage

*Kun Chang, Dongsheng Geng, Xifei Li, Jinli Yang, Yongji Tang, Mei Cai, Ruying Li, and Xueliang Sun**

The extensive range of possibilities for using a rechargeable lithium ion battery (LIB) for stationary power storage applications has stimulated significant research to improve its energy, power density and cycling life. The current use of graphite as a commercially available anode material cannot fully meet the energy density requirements for LIB applications in electric vehicles due to its relatively small capacity (372 mAh/g). In the next generation LIB, graphite should be replaced by alternative higher capacity materials and graphene based composite is one of the promising choices. The discovery of graphene has attracted wide-ranging interest due to its unique physical and chemical properties and potential for applications in electronic devices and sensors.[1–3] This has led to the development of a significant number of graphene-based materials for use as LIB anodes and results have been generally promising due to high specific capacity and improvement of its cycling ability. In recent years, chemical substitutional doping has been used to enhance the properties of graphene—further improving its properties beyond just morphology and size control. This includes the use of sulfur, boron, and nitrogen doping, the latter of which is particularly effective in modulating the electronic properties of graphene.[4–6] Based on these results, we expect that nitrogen-doped (N-doped) graphene will be used as a template for synthesis of active electrode materials.

Compared to graphene-based metal oxide materials, some graphene-based transition metal sulfides possess consummate 2D-layered structures. The matched structure between transition metal sulfides and graphene avoids the exfoliation of electrode materials and capacity fading during the charge/discharge process.[7–9] As a typical layered transition metal sulfide, MoS_2 has a structure similar to graphite, consisting of three atom layers of S-Mo-S stacked together through van der Waals interactions.[10,11] This layered structure enables the efficient intercalation and deintercalation of lithium ions. In recent years, many published reports have articulated various processes for preparing MoS_2 or MoS_2 composites as LIB anodes, which generally reach a reversible capacity of 800 ~ 900 mAh/g.[12–14] In our previous work, we reported a series of studies on MoS_2 with graphene composites that exhibited very high reversible capacity (1000 ~ 1200 mAh/g), excellent cyclic stability and high-rate capability.[7,8,15,16] However, deficiencies and questions remain concerning the use of MoS_2/graphene composites and graphene-based materials. For example, it is not well understood how MoS_2 nanoparticles are able to uniformly grow on the surface of graphene—MoO_4^{2-} anions, unlike metal cations, should be easily adsorbed on the graphene oxide (GO)—and why the reversible capacity increases gradually during the cycle.

Therefore, our current work presents a facile process for the synthesis of ultrathin MoS_2/N-doped graphene (MoS_2/N-G) nanosheets to reveal the growth mechanism of MoS_2 on the surface of N-doped graphene. The MoS_2/N-G composite exhibits exceptional high initial reversible capacity, outstanding cyclic stability and high-rate capability. In addition, using electrochemical impedance spectra (EIS) we explain the reason for rising capacity during the cycles that can occur in graphene-based materials.

The general view of MoS_2/N-G composite nanosheets is shown in **Figure 1** a. It can be seen that MoS_2/N-G composites consist of ultrathin 2D nanosheets with a diameter of ~100 nm. HRTEM images (Figure 1b and 1c) show that MoS_2 layers with an interlayer distance of 0.62 nm are grown on the surface of N-doped graphene. As shown in Figure S1 (see Supporting Information, SI), when comparing the morphology of MoS_2, MoS_2/G and MoS_2/N-G, it is found that MoS_2/N-G nanosheets are thinner than the others. This indicates that during the synthesis of MoS_2/G and MoS_2/N-G composites, graphene or N-doped graphene sheets greatly inhibit the restacking of MoS_2 layers. Moreover, compared to graphene and N-doped graphene (SI, Figure S1d, 1e), it is found that N-graphene possesses a rougher and more wrinkled surface than graphene. From Raman spectra of graphene and N-graphene in Figure S2c, it is known that the greater number of defect sites and vacancies exists in N-doped graphene[17,18] which allows MoS_2 particles to be more effectively and uniformly dispersed on its surface.

The same characteristic can be observed by X-ray diffraction (XRD) analysis as shown in Figure 1d. MoS_2/G and MoS_2/N-G show a crystalline structure similar to that of pure MoS_2, which is congruent with a hexagonal structure (JCPDS 37-1492). In addition, the XRD patterns of MoS_2/G and MoS_2/N-G show that growth of (002) plane was inhibited due to the incorporation of graphene or N-doped graphene. It is worth noting that the (002) diffraction peak of graphene or N-graphene cannot be detected (see SI Figure S2a and S2b), indicating that the graphene or N-graphene layers are divided by MoS_2 layers during

Dr. K. Chang, Dr. D. S. Geng, Dr. X. F. Li, J. L. Yang, Dr. Y. J. Tang, R. Y. Li, Prof. X. L. Sun
Nanomaterials and Energy Lab
Department of Mechanical and Materials Engineering
the University of Western Ontario
London, Ontario, N6A 5B9, Canada
E-mail: xsun@eng.uwo.ca
Dr. M. Cai
General Motors R&D Center
Warren, MI 48090-9055 USA

DOI: 10.1002/aenm.201201108

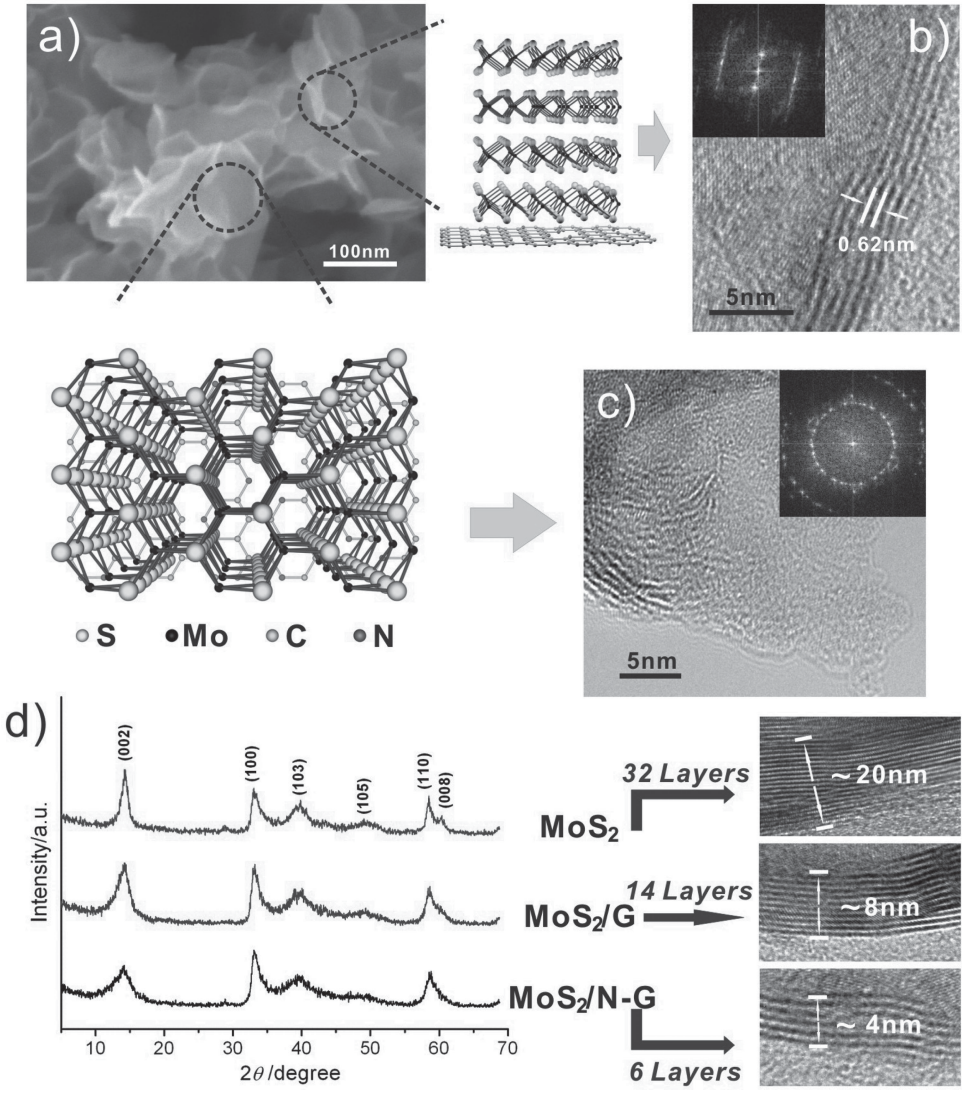

Figure 1. a) SEM image of ultrathin MoS_2/N-G nanosheets; b) HRTEM image of MoS_2/N-G nanosheet layers; c) HRTEM image of MoS_2/N-G nanosheet plane; insets show the Fast Fourier Transform (FFT) patterns of MoS_2/N-G nanosheet layers and plane; the figures on right and bottom of a) show the schematic illustrations of microstructure of MoS_2/N-G nanosheets; d) XRD patterns of pure MoS_2, MoS_2/graphene and MoS_2/N-G samples, and the corresponding HRTEM images of layer numbers.

the reaction route. According to the Scherrer equation ($D = K\lambda/\beta\cos\theta$), the average *c*-stacking height, calculated from the (002) reflection, is 20 nm for pure MoS_2, 8 nm for MoS_2/G and 4 nm for MoS_2/N-G. Based on the above, we can reasonably estimate the average number of layers for MoS_2/N-G to be 5 ~ 6—significantly less than that of MoS_2/G (8 ~ 9 layers) and pure MoS_2 (over 20 layers). This case also can be observed in the HRTEM images.

Regarding the growth mechanism of graphene-based materials, many references report that metal cations could be easily adsorbed on the surface of GO due to the existence of negative charges on its surface.[19] However, in our experiment, using Na_2MoO_4 as an initial material, MoS_2 particles were not able to disperse on the surface of graphene or N-graphene. Li *et al.*[20] demonstrated that GO nanosheets could be used as a novel substrate for the nucleation and subsequent growth of MoS_2 and found that MoS_2 growth is selective on GO. In our experiment, we found that two-step reactions occurred during the route. As shown in **Figure 2**a, a portion of L-cysteine is first decomposed to pure sulfur upon heating and anchored on the surface of N-graphene through nucleation, and then MoS_2 nanosheets subsequently formed in situ. This reaction can be shown using Energy-dispersive X-ray Spectroscopy (EDX) mapping and X-ray Photoelectron Spectroscopy (XPS) analysis of pure N-graphene using L-Cys (see SI, Figure S4 and S5). From the analysis of XPS (SI, Figure S5), it can be shown that the S element exists in the form of elemental sulfur.

Figures 2b to 2i show the growth mechanism of MoS_2/N-G composites. It can be seen that the N-graphene sheets with the thickness of 5 ~ 6 nm dispersed in the solution (Figures 2b, c and d) and there were no significant morphological changes observed when reacting for 2 h and 6 h (Figures 2e and 2f).

Adv. Energy Mater. **2013**,
DOI: 10.1002/aenm.201201108

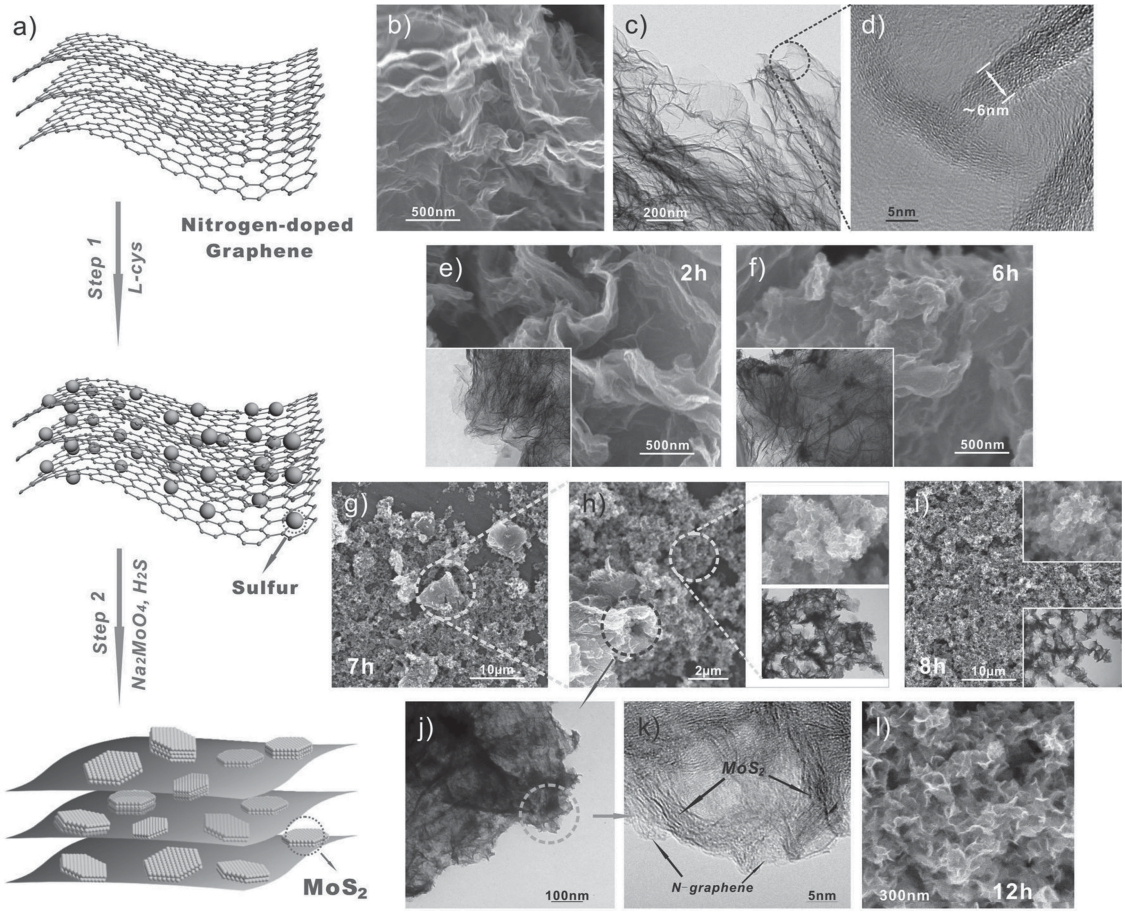

Figure 2. a) Schematic illustration of growth mechanism of MoS_2/N-G composite nanosheets; b) SEM image of N-doped graphene; c) TEM image of N-doped graphene; d) HRTEM image of N-doped graphene; e) SEM image of results reacting for 2 h, insert shows the corresponding TEM image; f) SEM image of results reacting for 6 h, insert shows the corresponding TEM image; g) SEM image of results reacting for 7 h; h) SEM image of partial enlargement of g); i) SEM image of results reacting for 8h, inserts show the SEM image (top) and TEM image (bottom) of partial enlargement; j) TEM image of partial enlargement of h); k) HRTEM image of partial enlargement of j); l) SEM image of results reacting for 12 h.

EDX mapping (SI, Figure S6) shows that the S element can be detected but not the Mo element—indicating no formation of MoS_2. When reacting for 7h, as shown in Figures 2g and 2 h, the coexistence of MoS_2/N-G and N-graphene can be observed. In Figures 2 j and 2 k, MoS_2 nanosheets can be seen growing uniformly on the surface of N-graphene. Subsequently, when reacting for 8 h, Figure 2i shows only MoS_2/N-G composites can be observed, indicating all of the products have transformed into the MoS_2/N-G composites. Completion of the reaction is achieved and the products obtained by reacting for 12 h, as shown in Figure 2i. Based on the growth mechanism of MoS_2/N-G (as shown in Figure 2), we can conclude that during the reaction, a portion of L-Cys is decomposed to sulfur nanoparticles and anchored on the surface of N-graphene through nucleation, resulting in the formation and growth of MoS_2 nanosheets. Finally, the remaining elemental sulfur is sublimed away during the annealing process. To determine the chemical composition of MoS_2/N-G composites, XPS measurements were carried out in the region of 0 ~ 1100 eV. **Figure 3**a shows that the sample contains the O, C, N, Mo and S elements and the atomic ratio of the elements is summarized in the insert of Figure 3a. The calculated atomic ratio of Mo to S element is 1 to 2, approaching the theoretical value of MoS_2. Also, it can be seen that a small quantity of O comes from a few parts of N-graphene that were not completely reduced during the hydrothermal and annealing processes. In Figure 3b, the high-resolution of C 1s, it can be seen that apart from most of the "C = C" bond, components of the oxygen-functional group still exist—including hydroxyl, epoxy, carbonyl and carboxyl. Figure 3c shows the high-resolution of S 2p, which contains S $2p_{3/2}$ at 162.6 eV and S $2p_{1/2}$ at 163.8 eV, indicating the products are stoichiometric MoS_2. As shown in Figure 3d, the weak N 1s signal is overlapped by the strong Mo $2p_{3/2}$ signal, resulting in challenges in extracting detailed information about N 1s. However, we can overcome this difficulty by considering Figure S5 (SI), which shows two peaks at 400.3 eV and 398.5 eV respectively. Several reports indicate that N-doping can actively enhance the properties of graphene, especially the electronic properties,[19,21] which are also presented in our studies.

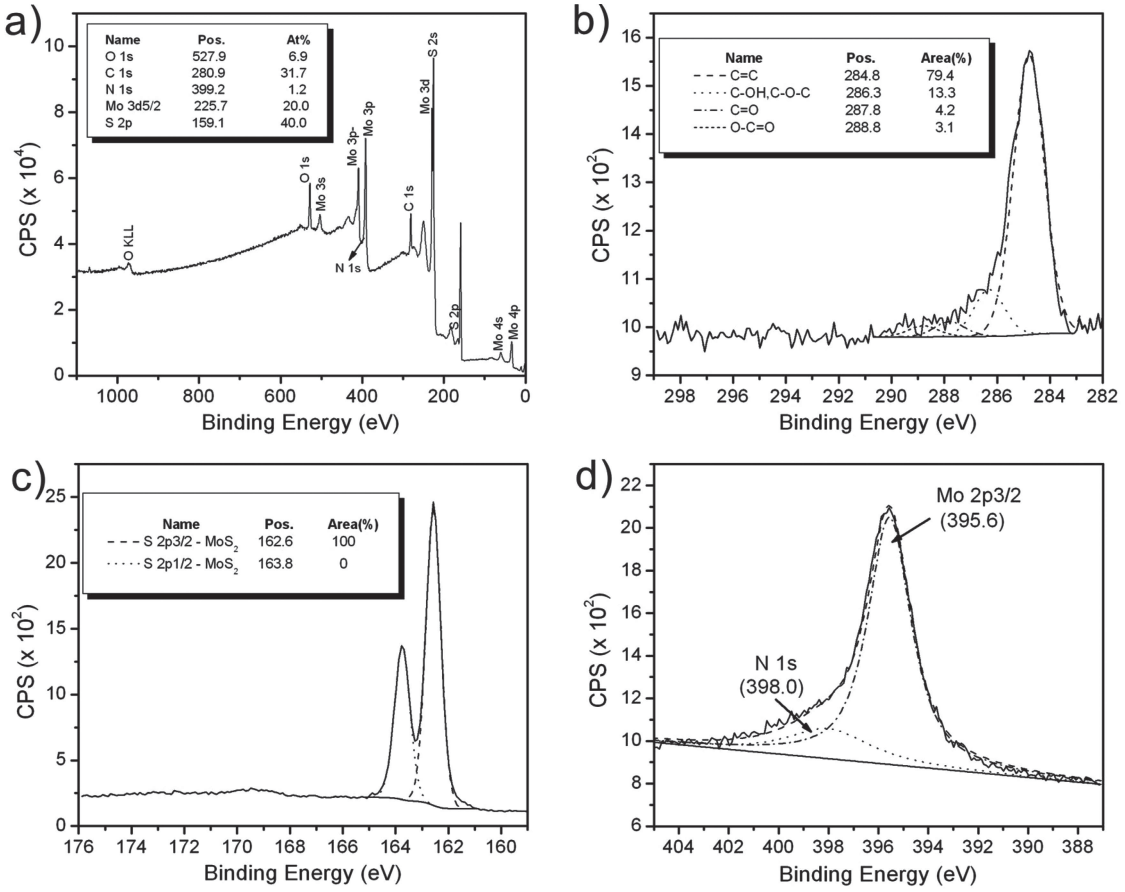

Figure 3. XPS patterns of MoS_2/N-G sample: a) survey and high-resolution of b) C 1s, c) S 2p and d) N 1s.

Figure 4 shows the electrochemical performance of MoS_2, MoS_2/G and MoS_2/N-G electrodes. From the first five cyclic voltammetry (CV) curves of MoS_2/N-G composite (Figure 4a), two reduction peaks at 1.1 V and 0.5 V and two oxidation peaks at 1.6 V and 2.3 V are observed during the first cycle. The reduction peak at 1.1 V can be attributed to Li insertion into the interlayers of MoS_2, accompanied by phase transformation from 2H to 1T structures of Li_xMoS_2.[22] The second pronounced reduction peak can be ascribed to the reduction of Li_xMoS_2 to Mo metal and Li_2S via a conversion reaction, and then the formation of a gel-like polymeric layer resulting from electrochemically driven electrolyte degradation. The oxidation peak at 1.6 V can be attributed to partial oxidation of Mo to form MoS_2 due to the defect sites leading to non-uniform delithiation. The second oxidation peak at 2.3 V is attributed to the formation of MoS_2. During the subsequent cycles, the reversible reaction based on the equation: $MoS_2 + 4Li \leftrightarrow Mo + 2Li_2S$, is accompanied by the redox of Mo nanoparticles and the reversible growth of the gel-like layer.[23] During subsequent discharge cycles, the potential plateau observed at 0.6 V disappeared with emergence of two new potential plateaus at 1.9 V and 1.2 V which is in agreement with previous observation in the literature.[24] As shown in Figure 4a and Figure S8, MoS_2/N-G and MoS_2/G electrodes have the similar peak current position and potential plateaus with pure MoS_2 (SI, Figure S7), indicating that graphene or N-graphene has no obvious potential plateaus. In comparison with MoS_2 (SI, Figure S7), the oxidation peaks at 2.3 V for MoS_2/N-G and MoS_2/G (SI, Figure S8) are not decreased during the cycling, indicating graphene and N-graphene can stabilize the electrode structure. As shown in Figure 4b, the MoS_2 electrode delivers an initial reversible capacity of 694.1 mAh/g. However, as the number of cycles increases, the capacity decreases—to 413.8 mAh/g after 50 cycles. In comparison, MoS_2/G and MoS_2/N-G electrodes exhibit much higher initial reversible capacities of 1005.5 mAh/g and 1021.2 mAh/g respectively, which show the stable cyclic behaviour during and after cycles. Interestingly, for the MoS_2/N-G electrode, the specific capacity increases during the cycle and can reach 1285.3 mAh/g after 50 cycles. Similar results have been reported in other studies and the reason for this phenomenon is still not known.[9,25,26] In our previous work,[27] we found that pure N-graphene exhibited a significant capacity increase during the cycle, which may be caused by more defect sites in N-graphene. In order to understand why the MoS_2/N-G electrode exhibited the rising capacity, alternating current impedance measurements were performed after 5, 20 and 40 cycles, as shown in Figure 4e (a detailed illustration can be seen in SI, Figure S9). Generally, it is well-known that the electrochemical surface area is proportional to

DOI: 10.1002/aenm.201201108

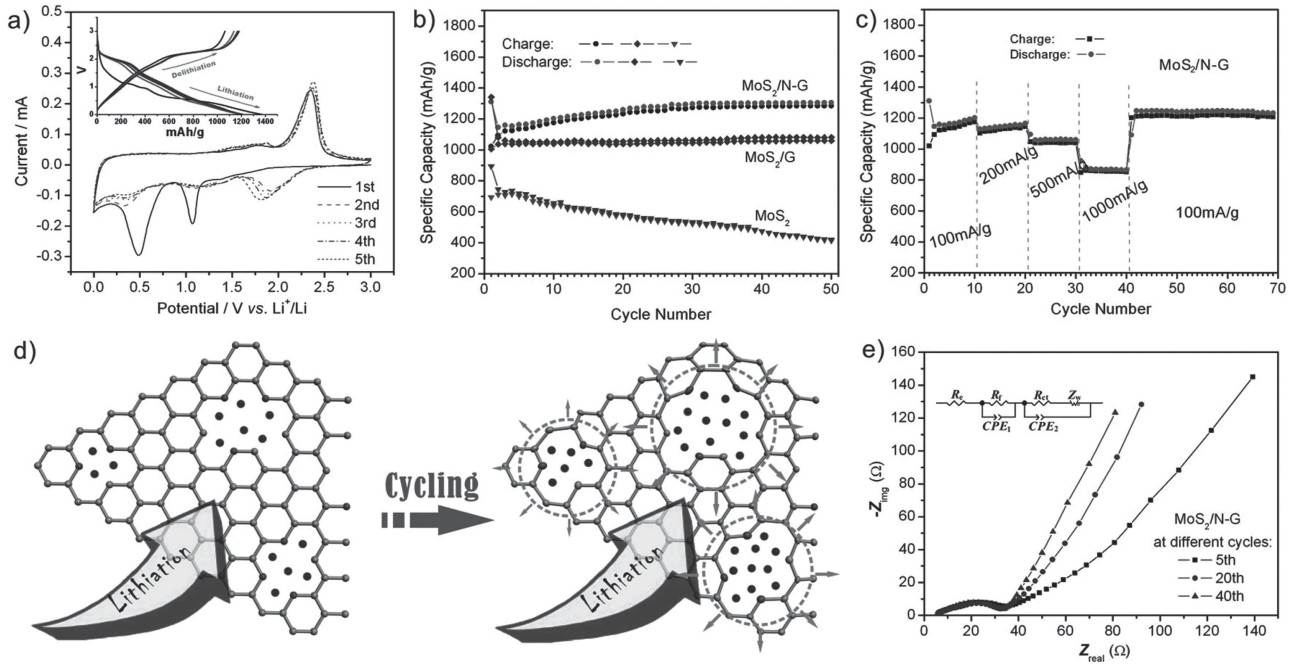

Figure 4. Electrochemical characterizations of a half-cell composed of different electrodes *vs.* Li foil: a) cyclic voltammogram of MoS_2/N-G at a scan rate of 0.1 mV during the first five cycles, insert shows the first five charge and discharge curves of MoS_2/N-G at a current density of 100 mAh/g, b) cycling behaviors of MoS_2, MoS_2/G and MoS_2/N-G samples at a current density of 100 mAh/g, c) cycling behavior of MoS_2/N-G electrode at various current densities; d) schematic illustration of N-doped graphene during the cycling: the defect sites or vacancies are extending gradually, facilitating more intercalation of Li^+ ions, blue balls represent Li^+ ions; e) Nyquist plots of the MoS_2, MoS_2/G and MoS_2/N-G electrodes obtained by applying a sine wave with amplitude of 5.0 mV over the frequency range from 200 KHz to 0.01 Hz; insert shows the equivalent circuit model of the studied system.

the capacitance of electrode/electrolyte interfaces. It was found that the capacitance value (see SI, Table S2) of the electrode increases during the cycle, which means the electrochemical surface area of the electrode increases. It is indicated that those defect sites and vacancies as Li^+ ions active sites would be extended gradually and thereby facilitated more intercalation of Li^+ ions. This conclusion is supported by Figure 4d. At the beginning of the lithiation process, the vacancies could trap a number of Li^+ ions. As the cycles increase, these vacancies are extended, facilitating the insertion of more Li^+ ions. Due to the increased number of defect sites and vacancies on N-graphene, the MoS_2/N-G composite shows rising capacity during the cycle, exhibiting excellent cyclic stability. In addition, the MoS_2/N-G electrode demonstrates good rate capability, as shown in Figure 4c. Even at a high current density of 1,000 mA/g, the specific capacity remains at 850 mAh/g—indicating that these novel composites could serve as promising anode materials for high-performance LIBs in a wide range of applications.

In summary, from the investigation of MoS_2/N-G composites, we revealed the growth mechanism of MoS_2 nanosheets on the surface of N-graphene. We also showed the reason for rising capacity during the cycle which is caused by extension of the defect sites and vacancies of the composites. This innovative MoS_2/N-G composite exhibits exceptional high capacity, superior cyclic stability and high-rate capability—which could be further explored for high-capacity and environmentally-friendly anode materials for LIB applications.

Experimental Section

Synthesis of graphene powder and nitrogen-doped graphene powder: Natural flake graphite (Aldrich, +100 mesh) was used as the starting material. Graphene was first prepared by the oxidation of graphite powder using the modified Hummers' method.[28] Typically, graphite powder (1 g) and sodium nitrate (0.75 g) were first stirred in concentrated sulphuric acid (37.5 mL) while being cooled in an ice water bath. Then potassium permanganate (4.5 g) was gradually added to form a new mixture. After 2 h in an ice water bath, the mixture was allowed to stand for five days at room temperature with gentle stirring. Thereafter, 100 mL of 5 wt% H_2SO_4 aqueous solution was added into the above mixture over 1 h with stirring. Then, 3 g of H_2O_2 (30 wt% aqueous solution) was also added to the above liquid and the mixture was stirred for 2 h. After that, the suspension was filtered and washed until the pH value of the filtrate was neutral. Finally, the dried graphite oxide was heated at 1050 °C for 30 s under Ar to get graphene.[29] Nitrogen doped graphene was further obtained by heating the graphene under high purity ammonia mixed with Ar at 900 °C for 4h.[30]

Synthesis of MoS_2, MoS_2/graphene and MoS_2/N-doped graphene: The mixture of 0.3 g of $Na_2MoO_4{\cdot}2H_2O$ and 0.48 g of L-cysteine were dissolved in 40 mL of DI water, and then transferred into a 50 mL Teflon-lined stainless steel autoclave, sealed tightly, and heated at 180 °C for 12 h. After cooling naturally, the black precipitates were collected by centrifugation, washed with DI water and ethanol, and dried in a vacuum oven at 80 °C for overnight. The black powder was annealed in a conventional tube furnace at 800 °C for 2 h in Ar atmosphere, and then the MoS_2 powder was obtained. With the same method as above, adding 0.030 g as-prepared graphene or N-doped graphene into the starting materials solution, the MoS_2/graphene or MoS_2/N-doped graphene powder could be obtained after annealing at 800 °C for 2 h in Ar atmosphere, respectively.

Characterizations: The samples were characterized by X-ray diffraction (XRD, Rigaku RU-200BVH diffractometer employing a Cu-K_α source), field emission scanning electron microscope (FESEM, Hitachi S-4800), transmission electron microscope (TEM, Hitachi H-7000), high-resolution transmission electron microscope (HRTEM, JEOL 2010F), X-ray photoelectron spectroscopy (XPS, Kratos Axis Ultra Al at 14 kV), energy dispersive X-ray spectroscopy (EDX, GENESIS 4000).

Electrochemical measurements: The electrochemical tests were measured using two-electrode coin cells assembled in an argon-filled glovebox. Lithium sheets as the counter electrode and reference electrode, and a polypropylene film (Celgard-2400) was used as a separator. The electrolyte was a 1.0M $LiPF_6$ solution in a mixture of ethylene carbonate/dimethyl carbonate (EC/DMC) (1:1 in volume). The working electrodes were prepared by a slurry coating procedure. The slurry consisted of 80 wt% active materials, 10 wt% acetylene black, and 10 wt% polyvinylidene fluorides dissolved in *N*-methyl-2-pyrrolidinone. This slurry was spread on copper foil, which acted as a current collector. The coated electrodes were dried at 80 °C for 24 h under vacuum and then pressed. Cyclic voltammetry tests were performed on a versatile multichannel potentiostat 3/Z (VMP3) at a scan rate of 0.1 mV/s over a potential range of 0 to 3.0 V(*vs.* Li^+/Li). Charge-discharge characteristics were tested galvanostatically between 0.01 and 3.0 V (*vs.* Li^+/Li) at room temperature using an Arbin BT-2000 Battery Test System. Alternating current impedance spectra (VMP3) were obtained by applying a sine wave with amplitude of 0.5 mV over the frequency range from 200 kHz to 0.01 kHz.

Supporting Information

Supporting Information is available from the Wiley Online Library or from the author.

Acknowledgements

This work is supported by Natural Sciences and Engineering Research Council of Canada (NSERC), General Motors of Canada, Canada Research Chair (CRC) Program, and the University of Western Ontario.

Received: December 25, 2012
Revised: January 28, 2013
Published online:

[1] K. S. Novoselov, A. K. Geim, S. V. Morozov, D. Jiang, Y. Zhang, S. V. Dubonos, I. V. Grigorieva, A. A. Firsov, *Science* **2004**, *306*, 666.
[2] A. K. Geim, *Science* **2009**, *324*, 1530.
[3] A. K. Geim, K. S. Novoselov, *Nat. Mater.* **2007**, *6*, 183.
[4] H. B. Wang, T. Maiyalagan, X. Wang, *Acs Catalysis* **2012**, *2*, 781.
[5] Z. Yang, Z. Yao, G. F. Li, G. Y. Fang, H. G. Nie, Z. Liu, X. M. Zhou, X. Chen, S. M. Huang, *Acs Nano* **2012**, *6*, 205.
[6] D. S. Geng, S. L. Yang, Y. Zhang, J. L. Yang, J. Liu, R. Y. Li, T. K. Sham, X. L. Sun, S. Y. Ye, S. Knights, *Appl. Surf. Sci.* **2011**, *257*, 9193.
[7] K. Chang, W. X. Chen, *Acs Nano* **2011**, *5*, 4720.
[8] K. Chang, W. X. Chen, *Chem. Commun.* **2011**, *47*, 4252.
[9] K. Chang, Z. Wang, G. C. Huang, H. Li, W. X. Chen, J. Y. Lee, *J. Power Sources* **2012**, *201*, 259.
[10] R. Tenne, L. Margulis, M. Genut, G. Hodes, *Nature* **1992**, *360*, 444.
[11] H. S. S. R. Matte, A. Gomathi, A. K. Manna, D. J. Late, R. Datta, S. K. Pati, C. N. R. Rao, *Angew. Chem.-Int. Ed.* **2010**, *49*, 4059.
[12] S. Q. Wang, X. Y. Jiang, H. Zheng, H. M. Wu, S. J. Kim, C. Q. Feng, *Nanosci. Nanotechnol. Letters* **2012**, *4*, 378.
[13] H. Hwang, H. Kim, J. Cho, *Nano Lett.* **2011**, *11*, 4826.
[14] S. K. Das, R. Mallavajula, N. Jayaprakash, L. A. Archer, *J. Mater. Chem.* **2012**, *22*, 12988.
[15] K. Chang, W. X. Chen, L. Ma, H. Li, H. Li, F. H. Huang, Z. D. Xu, Q. B. Zhang, J. Y. Lee, *J. Mater. Chem.* **2011**, *21*, 6251.
[16] K. Chang, W. X. Chen, *J. Mater. Chem.* **2011**, *21*, 17175.
[17] D. S. Geng, Y. Chen, Y. G. Chen, Y. L. Li, R. Y. Li, X. L. Sun, S. Y. Ye, S. Knights, *Energy Environ. Sci.* **2011**, *4*, 760.
[18] Y. L. Li, J. J. Wang, X. F. Li, D. S. Geng, R. Y. Li, X. L. Sun, *Chem. Commun.* **2011**, *47*, 9438.
[19] N. G. Sahoo, Y. Z. Pan, L. Li, S. H. Chan, *Adv. Mater.* **2012**, *24*, 4203.
[20] Y. G. Li, H. L. Wang, L. M. Xie, Y. Y. Liang, G. S. Hong, H. J. Dai, *J. Am. Chem. Soc.* **2011**, *133*, 7296.
[21] Z. Jin, J. Yao, C. Kittrell, J. M. Tour, *Acs Nano* **2011**, *5*, 4112.
[22] Q. Wang, J. H. Li, *J. Phys. Chem. C* **2007**, *111*, 1675.
[23] C. F. Zhang, Z. Y. Wang, Z. P. Guo, X. W. Lou, *ACS Appl. Mat. Interfaces* **2012**, *4*, 3765.
[24] C. F. Zhang, H. B. Wu, Z. P. Guo, X. W. Lou, *Electrochem. Commun.* **2012**, *20*, 7.
[25] Z. S. Wu, W. C. Ren, L. Wen, L. B. Gao, J. P. Zhao, Z. P. Chen, G. M. Zhou, F. Li, H. M. Cheng, *Acs Nano* **2010**, *4*, 3187.
[26] Y. M. Sun, X. L. Hu, W. Luo, Y. H. Huang, *Acs Nano* **2011**, *5*, 7100.
[27] X. F. Li, D. S. Geng, Y. Zhang, X. B. Meng, R. Y. Li, X. L. Sun, *Electrochem. Commun.* **2011**, *13*, 822.
[28] W. S. Hummers, R. E. Offeman, *J. Am. Chem. Soc.* **1958**, *80*, 1339.
[29] H. C. Schniepp, J. L. Li, M. J. McAllister, H. Sai, M. Herrera-Alonso, D. H. Adamson, R. K. Prud'homme, R. Car, D. A. Saville, I. A. Aksay, *J. Phys. Chem. B* **2006**, *110*, 8535.
[30] X. L. Li, H. L. Wang, J. T. Robinson, H. Sanchez, G. Diankov, H. J. Dai, *J. Am. Chem. Soc.* **2009**, *131*, 15939.